Japanese Journal of Radiology (2020) 38:1062–1074
https://doi.org/10.1007/s11604-020-01001-8

ORIGINAL ARTICLE

Correlation between imaging features and molecular subtypes of breast cancer in young women (≤30 years old)

Junlin Huang[1] · Qing Lin[1] · Chunxiao Cui[1] · Jie Fei[1] · Xiaohui Su[1] · Lili Li[1] · Jinzhu Ma[1] · Min Zhang[1]

Received: 22 April 2020 / Accepted: 8 June 2020 / Published online: 19 June 2020

Abstract

Objectives To analyze the features of digital mammography (DM) plus digital breast tomosynthesis (DBT), ultrasonography (US) and magnetic resonance imaging (MRI) of breast cancer in young women (≤30 years old) and the correlation with molecular subtypes.

Materials and methods We performed a retrospective study of imaging features of consecutive young women aged ≤30 years who were treated and surgically confirmed with breast cancer between January 2013 and December 2019 in our institution. All patients were Chinese women. DM + DBT and US were available for 170 lesions, MRI for 41 lesions. The imaging features were analysed by univariate and multivariate logistic regression analyses to find the predictive factors of the molecular subtypes.

Results The predictive factors of the luminal B(HER2−) subtype ($n = 51$) were the mass with microcalcifications, irregular shape, spiculated margins, and shadowing posterior features (all $P < 0.01$). The predictive factors of the luminal B(HER2+) subtype ($n = 26$) were the spiculated margins (DBT + DM), angular margins (US), shadowing posterior features, and high vascularity (all $P < 0.05$). The predictive factors of the luminal A subtype ($n = 37$) were the mass without microcalcifications, spiculated margins, shadowing posterior features, and low vascularity (all $P < 0.05$). The predictive factors of the triple-negative subtype ($n = 31$) were the mass without microcalcifications, oval/round shape, circumscribed margins, enhancement of posterior features, and rim enhancement (MRI) (all $P < 0.005$). The predictive factors of the human-epidermal-growth-factor-receptor-2-enriched subtype ($n = 26$) were the only microcalcifications, microlobulated margins, and combined posterior feature (all $P < 0.05$).

Conclusion Compared with the general population of breast cancer, this young female population presents a different molecular phenotype distribution. Some imaging features of breast cancer in young women ≤30 years old can be used to predict certain tumor molecular subtypes.

Keywords Breast cancer · Young women · Tomosynthesis · Ultrasonography · Molecular subtypes

Introduction

Breast cancer in young women under 30 years of age is rare. However, the incidence rate of breast cancer increased significantly after 20 years old and the 5-year survival rate decreased [1, 2]. The incidence of breast cancer among young women (≤30-year-old) is <1% in Western countries [3], but more than 3% in Asian countries [4]. But, because of the huge population base of China, the number of female breast cancer cases is at the forefront of the world [5].

The clinical manifestation, treatment response, and prognosis of different molecular subtypes of breast cancer are significantly different [6, 7], so the preoperative identification of molecular subtypes of breast cancer is of great significance for the early specific treatment, which may prolong survival time of patients. Although biopsy is the gold standard for pathological evaluation, it is invasive. Therefore, it would be better if the molecular subtypes could be identified by noninvasive imaging diagnostic methods.

✉ Qing Lin
linqing9180@126.com

Junlin Huang
253237335@qq.com

[1] Department of Breast Radiology, Affiliated Hospital of Qingdao University, Qingdao University, No. 16, Jiangsu Road, Qingdao 266100, Shandong Province, China

Mammography is widely used to diagnose breast cancer. However, young women have dense breast parenchyma, which could reduce the sensitivity and accuracy of digital mammography (DM) [6, 8, 9]. Digital breast tomosynthesis (DBT) is a pseudo-3D imaging technique of the breast. DBT can reduce the masking effect of overlapping fibroglandular tissue, result in better discrimination of tissue structures, thereby potentially improve the visibility of the lesions [6, 8, 9]. Although digital breast tomosynthesis (DBT) has been used for clinical and screening diagnosis in Western countries, the application of DBT for clinical diagnosis is at an early stage in China due to the shortage of DBT equipment.

Breast cancer in young women under 40 or 35 years has attracted widespread attention, because young women have been excluded from standard screening programs and few studies have focused on imaging features of breast cancer in women aged below 30 years. In addition, there have been no published study of the application of DBT in distinguishing molecular subtypes of breast cancer in this age group. In this study, we evaluated the imaging features of breast cancer and correlated with the molecular subtypes in this young group to find more predictive imaging features.

Material and methods

Patients

The Institutional Review Board authorized this retrospective study, and the informed consent requirement was waived. All patients were Chinese women. The medical records of consecutive women who were diagnosed with breast cancer and treated at our institution between January 2013 and December 2019 were reviewed. All mammography and MRI (magnetic resonance imaging) images were retrieved from the picture archiving and communication system (PACS) (Centricity PACS Radiology RA1000 Workstation, General Electric, Milwaukee, WI, USA) at our institution. The clinical and histopathologic findings were extracted from the Hospital Information System (HIS) database at our institution.

In total, 168 patients (166 unilateral cases, two bilateral cases) under 30 years of age were included in this study. The median ages were 28 years old (20–30). Reasons for the initial examination included a palpable mass (131 cases; 77.9%), nipple discharge (23 cases; 13.7%), breast pain (8 cases; 4.8%), and family history of breast cancer in first or second relatives (6 cases; 3.6%). Three patients underwent next generation sequencing (NGS)-based BRCA1/BRCA2 mutation testing, and all results were benign variation. Besides, 25 patients underwent neoadjuvant chemotherapy, of which eight patients had no change, 17 patients had improvement, but there were no pCR (pathologic complete response) results. Mammography and ultrasound were available for 170 lesions, and MRI for 41 lesions.

Imaging equipment

Ultrasonography images of each breast were obtained using a 10–14 MHz linear probe (Acuson S2000, Siemens; EBU 7500, Siemens AG, Munich, Germany).

DBT and DM images were simultaneously acquired using the Hologic Selenia Dimensions mammography (Marlborough, MA, USA) equipment with combo mode. The X-ray tube rotated through an angular range of 15° (−7.5° to +7.5°) with the standard compression of the breast, which was then reconstructed into a series of section separation images of 1 mm. Standard two-view (mediolateral oblique and craniocaudal view) images were obtained on the affected side, and additional views were added if necessary.

All patients underwent MRI using the 3.0 T system (Siemens Skyra) with a dedicated 4-channel breast coil. The conventional sequences consisted of axial T1-weighted images (TR: 6 ms, TE: 2.46 ms, slice thickness 1.6 mm, 280 mm field of view, matrix 280 × 280), axial T2-weighted images (TR: 3000 ms, TE: 68 ms, slice thickness 1.6 mm, matrix 280 × 280), sagittal T2-weighted images (TR: 3000 ms, TE: 66 ms, slice thickness 1.6 mm, matrix 280 × 280), and diffuse-weighted images (TR: 5000 ms, TE: 68 ms, layer thickness 6.0 mm). For each dynamic enhancement study, eight sequences were obtained (one sequence per 60 s) after intravenous bolus injection of 0.2 mmol/kg Gd-DPTA, and a subtraction image was created for each sequence. After the dynamic enhancement, a coronal T1W fat-suppressed sequence was obtained. The time signal intensity curve (TIC) was drawn in the Aurora CADTM workstation. TIC was divided into three types: type 1 (persistent type), the signal strength continues to rise more than 10%; type 2 (plateau type), after the signal strength rises, it remains rising or falling within 10%; type 3 (washout type), it strengthened quickly in the early stage, and the signal decreased rapidly after reaching the peak, exceeding 10% of the peak intensity.

Image interpretation

All imaging features were retrospectively reviewed according to the American College of Radiology (ACR) Breast Imaging Reporting and Data System (BI-RADS) lexicon, 5th edition [10]. Each breast with more than one breast lesion was included in the analysis only once; their highest assessment was used to guarantee statistical independence of each observation. The classification of mammary gland composition was determined according to the DM image: "almost entirely fatty (ACR a)" and "scattered fibroglandular densities (ACR b)" were classified as non-dense breasts,

and "heterogeneously dense (ACR c)" and "extremely dense (ACR d)" breast tissue were classified as dense breasts.

For ultrasonography, lesions were classified as masses and intraductal calcifications. Analysis of mass lesions included shape, margins, echo patterns, posterior features, and Doppler vascularity. As to mammography, shape, margins, and density were analyzed in mass lesions, while assessing the shape and distribution of the isolated microcalcifications. For MRI imaging, internal enhancement, T2 signal intensity, and kinetic enhancement curves were analyzed in all lesions, while assessing the shape and margins of the mass lesions and the distribution of the non-mass lesions.

The images were analyzed by two radiologists with 2–8 years of experience in mammography, breast MRI diagnosis and breast ultrasound diagnosis. The retrospective double-blind method was used. All readers respectively reviewed the imaging after reaching consensus and were blinded to the outcome, including pathologic outcomes and other readers' interpretations. If the findings of DBT and DM were not consistent in an identical lesion, the DBT imaging feature was used as the final result for mass lesions and DM imaging feature was used for the distribution of microcalcifications. When the descriptions of the same imaging modality were inconsistent among the radiologists, a consensus was reached through discussion.

Histopathological analysis

Histologic subtype findings were classified as invasive ductal carcinomas (135 lesions; 79.4%), ductal carcinoma in situ (19 lesions; 11.2%), mucinous carcinoma (5 lesions), micropapillary carcinoma (5 lesions), metaplastic carcinoma (3 lesions), malignant phyllodes tumor (1 lesion), and small cell neuroendocrine carcinoma (1 lesion). The pathology report for each surgical specimen was used as the gold standard.

Molecular subtypes were defined according to the 2015 revised St. Gallen International Expert Consensus Recommendation [11]. Molecular subtypes were based on the expressions estrogen-receptor (ER), progesterone-receptor (PR), human epidermal growth factor receptor 2 (HER-2), and Ki-67 status. Regarding the HER2 assessment, tumors with a score of 3+ were classified as HER2 positive, while tumors with a score of 0 or 1+ were classified as negative. In tumors with a score of 2+, FISH analysis was used for gene amplification to determine the status of HER2. Cancers were categorized as luminal A(LA) (ER+, PR ≥ 20%, Ki-67 ≤ 20%, and HER2−); luminal B(LB) (HER2+) (ER+, HER2+, any Ki-67 value, any PR value); luminal B(LB) (HER2−) (ER+, HER2−, at least one of Ki-67 > 20% or PR < 20%); HER2-enriched (ER−, PR−, HER2+); and triple negative (TN) (ER−, PR− and HER2−).

In this study, LB(HER2−) subtype accounted for 52 (30.6%) cases, LB(HER2 +) subtype for 26 (15.3%), LA subtype for 37 (21.8%), TN subtype for 31 (18.2%) and HER2-enriched subtype for 24 (14.1%).

Statistical analysis

All statistical analyses were performed with SPSS software (version 22.0; SPSS Inc., Chicago, IL, USA) and SAS version 9.4 (SAS Institute, Cary, NC, USA). Descriptive statistics were reported with means or median of normal distribution data. Chi-square test or Fisher's exact test was used to evaluate the qualitative data. Bonferroni corrections were used for multiple comparisons [Pcorrection (P_c) = P value × 10 (times of comparisons among five subtypes)]. Then, the parameters that were found to be significant were analyzed using the univariate and multivariate logistic regression analyses with a forward stepwise selection method to estimate odds ratios (OR), associated 95% confidence interval (CI). P or $P_c < 0.05$ was considered statistically significant.

We finally used Cohen's kappa statistic to evaluate the pairwise agreement between two radiologists in terms of imaging features. The following as standards for strength of agreement: 0.01–0.20 = slight; 0.21–0.40 = fair; 0.41–0.60 = moderate; 0.61–0.80 = substantial; 0.81–0.99 = almost perfect; 1.0 = perfect [12].

Results

Imaging features

Ultrasound (US) features (Table 1)

Ultrasound detected 98.8% of the lesions and 2 cases of DCIS presented as microcalcifications were missed. The mass without microcalcifications case was the most frequent type (48.8%). For mass lesions, the most commonly detected features were the irregular shape (69.7%), hypoechogenicity (64.1%), spiculated margins (33.1%), shadowing posterior features (40.0%), and high vascularity (60.7%). Shadowing posterior feature was more recurrent and showed in LB(HER2−), LB(HER2+), LA subtypes than TN subtype (all $P_c < 0.005$). No statistically significant difference was found in echogenicity ($P = 0.474$) among the five subtypes. Low vascularity was more commonly observed in LA and TN subtypes than LB(HER2−) subtype (all $P_c < 0.05$).

Digital Mammography (DM) + Digital Breast Tomosynthesis (DBT) features (Table 2)

In 91.7% of patients, the parenchyma showed dense breasts (ACR c or d). More than half of the cases (78.3%) were mass lesions; among these, a mass without microcalcifications

was visible in 36.5% (62/170) of cases, a mass with microcalcifications was detected in 41.8% (71/170) of cases. Besides, eight cases showed no abnormality, of which six had extremely dense breast.

For the mass lesions, the most common findings were the irregular shape (74.4%), hyperdense mass (54.9%), and spiculated margins (52.6%). For the microcalcifications, the most common findings were the fine linear or linear branching microcalcifications (51.7%) and linear or segmental distribution (41.4%).

MRI features (Table 3)

All cases (100%) represented abnormal contrast enhancement. 80.5% (33/41) of cases presented as mass enhancement. Iso-intensity (78.0%) was the most frequently T2WI intensity. The kinetic curve pattern was mostly the washout type (56.1%).

For the mass lesions, the most frequent findings were the irregular shape (75.8%), spiculated margins (45.5%), and heterogenous enhancement pattern (66.7%). For the non-mass lesions, those were clumped enhancement (75.0%) and linear or segmental distribution (62.5%).

Univariate and multivariate logistic regression analyses (Table 4)

By univariate logistic regression analysis, the predictive factors of the LB(HER2−) subtype were mass with microcalcifications (OR = 2.88, $P = 0.002$) and spiculated

Table 1 Ultrasonography features of breast cancer in young women according to molecular subtypes

	Luminal B(HER2−) *n* (%)	Luminal B(HER2+) *n* (%)	Luminal A *n* (%)	Triple negative *n* (%)	HER-2 enriched *n* (%)	All cancer *n* (%)	#*P* value
Abnormality							< 0.001*
No abnormality	1 (1.9)	0	1 (2.7)	0	0	2 (1.2)	
Mass only	18 (34.6)	10 (38.5)	28 (75.7)	20 (64.5)	7 (29.2)	83 (48.8)	
Mass with microcalcifications	28 (53.8)	13 (50.0)	3 (8.1)	9 (29.0)	9 (37.5)	62 (36.5)	
Intraductal calcifications	5 (9.6)	3 (11.5)	5 (13.5)	2 (6.5)	8 (33.3)	23 (13.5)	
Shape (for mass)							< 0.001**
Oval/round	9 (19.6)	3 (13.0)	9 (29.0)	19 (65.5)	4 (25.0)	44 (30.3)	
Irregular	37 (80.4)	20 (87.0)	22 (71.0)	10 (34.5)	12 (75.0)	101 (69.7)	
Margins (for mass)							< 0.001*
Circumscribed	2 (4.3)	1 (4.3)	2 (6.5)	13 (44.8)	0	18 (12.4)	
Indistinct	13 (28.3)	6 (26.1)	7 (22.6)	6 (20.7)	4 (25.0)	36 (24.8)	
Microlobulated	3 (6.5)	1 (4.3)	3 (9.7)	6 (20.7)	7 (43.8)	20 (13.8)	
Spiculated	26 (56.5)	6 (26.1)	13 (41.9)	1 (3.4)	2 (12.5)	48 (33.1)	
Angular	2 (4.3)	9 (39.1)	6 (19.4)	3 (10.3)	3 (18.8)	23 (15.9)	
Echogenicity							0.474*
Hypoechoic	27 (58.7)	14 (60.9)	25 (80.6)	17 (58.6)	10 (62.5)	93 (64.1)	
Heterogenous	17 (37.0)	8 (34.8)	5 (16.1)	9 (31.0)	6 (37.5)	45 (31.0)	
Complex cystic and solid	2 (4.3)	1 (4.3)	1 (3.2)	3 (10.3)	0	7 (4.8)	
Posterior feature							< 0.001*
No	16 (34.8)	9 (39.1)	10 (32.3)	9 (31.0)	2 (12.5)	46 (31.7)	
Enhancement	4 (8.7)	0	1 (3.2)	16 (55.2)	3 (18.8)	24 (16.6)	
Shadowing	23 (50.0)	13 (56.5)	17 (54.8)	3 (10.3)	2 (12.5)	58 (40.0)	
Combined	3 (6.5)	1 (4.3)	3 (9.7)	1 (3.4)	9 (56.2)	17 (11.7)	
Vascularity							< 0.001*
Absent	1 (2.0)	0	2 (5.6)	2 (6.5)	0	5 (3.0)	
Low	14 (27.5)	3 (11.5)	22 (61.6)	14 (23.0)	8 (33.3)	61 (36.3)	
High	36 (70.6)	23 (88.5)	12 (33.3)	15 (48.4)	16 (66.7)	102 (60.7)	

Values in parentheses are percentages

*Fisher's exact test, **χ^2 test

#*P* values are calculated by the overall difference among the five subtypes

Table 2 DM + DBT features of breast cancer in young women according to molecular subtypes

	Luminal B(HER2−) *n* (%)	Luminal B(HER2+) *n* (%)	Luminal A *n* (%)	Triple negative *n* (%)	HER-2 enriched *n* (%)	All cancer *n* (%)	#*P* value
Breast density							0.734*
a, b	4 (7.8)	3 (11.5)	2 (5.6)	4 (12.9)	1 (4.2)	14 (8.3)	
c, d	47 (92.2)	23 (88.5)	34 (94.4)	27 (87.1)	23 (95.8)	154 (91.7)	
Abnormality							< 0.001*
No abnormality	0	1 (3.8)	6 (16.2)	0	1 (4.2)	8 (4.7)	
Mass only	12 (23.1)	6 (23.1)	19 (51.4)	19 (61.3)	6 (25.0)	62 (36.5)	
Mass with microcalcifications	31 (59.6)	15 (57.7)	6 (16.2)	10 (32.3)	9 (37.5)	71 (41.8)	
Microcalcifications only	9 (17.3)	4 (15.4)	6 (16.2)	2 (6.5)	8 (33.3)	29 (17.1)	
Shape (for mass)							< 0.001**
Oval/round	4 (9.3)	3 (14.3)	4 (16.0)	22 (75.9)	1 (6.7)	34 (25.6)	
Irregular	39 (90.7)	18 (85.7)	21 (84.0)	7 (24.1)	14 (93.3)	99 (74.4)	
Margins (for mass)							< 0.001*
Circumscribed	1 (2.3)	1 (4.8)	2 (8.0)	15 (51.7)	0	19 (14.3)	
Indistinct	7 (16.3)	3 (14.3)	3 (12.0)	3 (12.0)	4 (26.7)	20 (15.0)	
Microlobulated	6 (14.0)	1 (4.8)	2 (8.0)	7 (24.1)	8 (53.3)	24 (18.0)	
Spiculated	29 (67.4)	16 (76.2)	18 (24.0)	4 (13.8)	3 (20.0)	70 (52.6)	
Density (for mass)							0.115**
Hyper	21 (48.8)	9 (42.9)	12 (48.0)	19 (65.5)	12 (80.0)	73 (54.9)	
Iso	22 (51.2)	12 (57.1)	13 (52.0)	10 (34.5)	3 (20.0)	60 (45.1)	
Shape (for calcifications)							0.364*
Amorphous	2 (22.2)	0	0	0	0	2 (6.9)	
Fine pleomorphic or coarse heterogeneous	5 (55.6)	2 (50.0)	3 (50.0)	0	2 (25.0)	12 (41.4)	
Fine linear or linear branching	2 (22.2)	2 (50.0)	3 (50.0)	2 (100.0)	6 (75.0)	15 (51.7)	
Distribution (for calcifications)							0.679*
Diffuse	1 (11.1)	0	0	1 (50.0)	1 (12.5)	3 (10.3)	
Regional	2 (22.2)	0	1 (16.7)	0	1 (12.5)	4 (13.8)	
Grouped	3 (33.3)	3 (75.0)	3 (50.0)	0	1 (12.5)	10 (34.5)	
Linear/segmental	3 (33.3)	1 (25.0)	2 (33.3)	1 (50.0)	5 (62.5)	12 (41.4)	

Values in parentheses are percentages

DBT digital breast tomosynthesis, *DM* digital mammography

**χ^2 test; *Fisher's exact test

#*P* values are calculated by the overall difference among the five subtypes

margins (OR = 4.56, $P < 0.001$) in US; mass with microcalcifications (OR = 2.88, $P = 0.002$), irregular shape (OR = 4.88, $P = 0.006$), and spiculated margins (OR = 2.48, $P = 0.02$) in DBT + DM (Fig. 1). The predictive factors of the LB(HER2+) subtype were angular margins (OR = 4.96, $P = 0.002$) and high vascularity (OR = 6.11, $P = 0.004$) in US; spiculated margins (OR = 3.44, $P = 0.024$) in DBT + DM (Fig. 2). The predictive factors of the LA subtype were mass without microcalcifications (OR = 4.90, $P < 0.001$) and low vascularity (OR = 3.75, $P = 0.001$) in US; no abnormality (OR = 12.68, $P = 0.003$), mass without microcalcifications (OR = 2.21, $P = 0.036$), and spiculated margins (OR = 2.77, $P = 0.036$) in DBT + DM (Fig. 3). The predictive factors of the TN subtype were oval/round shape (OR = 6.92), circumscribed margins (OR = 18.04), and enhancement of posterior feature (OR = 16.62) (all $P < 0.001$) in US; mass without microcalcifications (OR = 3.54, $P = 0.002$), oval/round shape (OR = 24.10), and circumscribed margins (OR = 26.79) (all $P < 0.001$) in DBT + DM; oval/round shape, circumscribed margins (all OR = 40.00), and rim

Table 3 MRI features of breast cancer in young women according to molecular subtypes

	Luminal B(HER2−) *n* (%)	Luminal B(HER2+) *n* (%)	Luminal A *n* (%)	Triple negative *n* (%)	HER-2 enriched *n* (%)	All cancer *n* (%)	#*P* value
Lesion type							0.886*
Mass	9 (75.0)	5 (83.3)	8 (72.7)	6 (100.0)	5 (83.3)	33 (80.5)	
Non-mass	3 (25.0)	1 (16.7)	3 (27.3)	0	1 (16.7)	8 (19.5)	
Mass							
Shape							0.005*
Oval/round	2 (22.2)	0	1 (12.5)	5 (83.3)	0	8 (24.4)	
Irregular	7 (77.8)	5 (100.0)	7 (87.5)	1 (16.7)	5 (100.0)	25 (75.8)	
Margins							0.012*
Circumscribed	2 (22.2)	0	1 (12.5)	5 (83.3)	0	8 (24.4)	
Irregular	4 (44.4)	1 (20.0)	1 (12.5)	1 (16.7)	3 (60.0)	10 (30.3)	
Spiculated	3 (33.3)	4 (80.0)	6 (5.0)	0	2 (40.0)	15 (45.5)	
Enhancement							0.001*
Homogenous	1 (11.1)	0	1 (12.5)	0	1 (20.0)	3 (9.1)	
Heterogenous	7 (77.8)	4 (80.0)	7 (87.5)	0	4 (80.0)	22 (66.7)	
Rim	1 (11.1)	1 (20.0)	0	6 (100.0)	0	8 (24.3)	
NME							
Distribution							1.000*
Focal/regional	1 (33.3)	0	1 (33.3)	0	0	2 (25.0)	
Linear/segmental	1 (33.3)	1 (100.0)	2 (66.6)	0	1 (100.0)	5 (62.5)	
Diffuse	1 (33.3)	0	0	0	0	1 (12.5)	
Enhancement							0.464*
Heterogenous	0	1 (100.0)	0	0	0	1 (12.5)	
Clumped	3 (100.0)	0	2 (66.6)	0	1 (100.0)	6 (75.0)	
Clustered ring	0	0	1 (33.3)	0	0	1 (12.5)	
T2 signal intensity							0.007*
Iso	10 (83.3)	5 (83.3)	10 (90.9)	1 (16.7)	6 (100.0)	32 (78.0)	
Mixed	1 (8.3)	1 (16.7)	0	4 (66.7)	0	6 (14.6)	
High	1 (8.3)	0	1 (9.1)	1 (16.7)	0	3 (7.3)	
Kinetics							0.448*
Type 2 (plateau)	5 (41.7)	3 (50.0)	7 (63.6)	1 (16.7)	2 (33.3)	18 (43.9)	
Type 3 (washout)	7 (58.3)	3 (50.0)	4 (36.4)	5 (83.3)	4 (66.7)	23 (56.1)	

Values in parentheses are percentages

*Fisher's exact test

#*P* values are calculated by the overall difference among the five subtypes

enhancement (OR = 132.60) (all $P = 0.003$) in MRI (Fig. 4). The predictive factors of the HER2-enriched subtype were only microcalcifications (OR = 4.37, $P = 0.004$), microlobulated margins (OR = 6.94, $P = 0.001$), and combined posterior feature (OR = 19.45, $P < 0.001$) in US; only microcalcifications (OR = 2.98, $P = 0.027$) and microlobulated margins (OR = 7.29, $P = 0.001$) in DBT + DM (Fig. 5).

By multivariate logistic regression analysis, spiculated margins in US (OR = 4.62, P < 0.001) was the strongest independent predictor for LB(HER2−) subtype; no abnormality (missed diagnosis) in DBT + DM (OR = 22.00, $P < 0.001$) was for LA subtype; enhanced posterior feature in US (OR = 9.96) and oval/round shape (OR = 13.49) (all $P < 0.001$) in DBT + DM were for TN subtype; combined posterior feature (OR = 31.90, $P < 0.001$) in US was for HER2-enriched subtype.

Agreement between radiologist in evaluating imaging findings (Table 5)

In all cases, we observed substantial to almost perfect agreement (kappa values ranged from 0.61 to 0.99).

Table 4 Univariate and multivariate logistic regression analysis

Univariate logistic regression analysis		*P* values	Multivariate logistic regression analysis		*P* values
	OR (95% CI)			OR (95% CI)	
Luminal B(HER2−)					
Mass with microcalcifications (US)	2.88 (1.47–5.66)	0.002	Mass with microcalcifications (US)	3.04 (1.40–6.56)	0.005
Spiculated margins (US)	4.56 (2.15–9.64)	< 0.001	Spiculated margins (US)	4.62 (2.12–10.09)	< 0.001
Mass with microcalcifications (DBT + DM)	2.88 (1.47–5.64)	0.002	Mass with microcalcifications (DBT + DM)	2.65 (1.18–5.97)	0.018
Irregular shape (DBT + DM)	4.88 (1.59–14.92)	0.006	Irregular shape (DBT + DM)	3.91 (1.25–12.27)	0.019
Spiculated margins (DBT + DM)	2.48 (1.16–5.30)	0.02	Spiculated margins (DBT + DM)		0.256
Luminal B(HER2+)					
Angular margins (US)	4.96 (1.81–13.56)	0.002	Angular margins (US)	6.47 (2.13–19.62)	0.001
High vascularity (US)	6.11 (1.76–21.29)	0.004	High vascularity (US)	6.73 (1.76–25.74)	0.005
Spiculated margins (DBT + DM)	3.44 (1.18–10.02)	0.024			
Luminal A					
Mass (US)	4.90 (2.08–11.56)	< 0.001	Mass (US)	4.10 (1.70–9.87)	0.002
Low vascularity (US)	3.75 (1.74–8.07)	0.001	Low vascularity (US)	3.02 (1.36–6.70)	0.007
No abnormality (DBT + DM)	12.68 (2.44–65.85)	0.003	No abnormality (DBT + DM)	22.00 (3.98–121.66)	< 0.001
Mass (DBT + DM)	2.21 (1.05–4.63)	0.036	Mass (DBT + DM)	3.24 (1.44–7.28)	0.004
Spiculated margins (DBT + DM)	2.77 (1.07–7.17)	0.036	Spiculated margins (DBT + DM)	3.99 (1.41–11.28)	0.009
TN					
Oval/round shape (US)	6.92 (2.86–16.75)	< 0.001	Oval/round shape (US)	3.52 (1.19–10.40)	0.023
Circumscribed margins (US)	18.04 (5.67–57.36)	< 0.001	Circumscribed margins (US)	6.48 (1.65–25.43)	0.007
Enhancement of posterior feature (US)	16.62 (5.96–46.33)	< 0.001	Enhancement of posterior feature (US)	9.96 (3.13–31.71)	< 0.001
Mass (DBT + DM)	3.54 (1.58–7.92)	0.002	Mass (DBT + DM)		0.735
Oval/round shape (DBT + DM)	24.10 (8.50–68.29)	< 0.001	Oval/round shape (DBT + DM)	13.49 (4.37–41.49)	< 0.001
Circumscribed margins (DBT + DM)	26.79 (7.78–92.25)	< 0.001	Circumscribed margins (DBT + DM)	10.52 (2.52–43.92)	0.001
Oval/round shape (MRI)	40.00 (3.42–468.07)	0.003	Oval/round shape (MRI)		0.087
Circumscribed margins (MRI)	40.00 (3.42–468.07)	0.003	Circumscribed margins (MRI)		0.087
Rim enhancement (MRI)	132.60 (5.16–>999.99)	0.003	Rim enhancement (MRI)	76.29 (2.44–> 999.99)	0.014
HER2-enriched					
Microlobulated margins (US)	6.94 (2.22–21.74)	0.001	Microlobulated margins (US)	13.19 (2.90–59.948)	0.001
Combined posterior feature (US)	19.45 (5.74–65.85)	< 0.001	Combined posterior feature (US)	31.90 (7.18–141.69)	< 0.001
Microcalcifications (US)	4.37 (1.60–11.90)	0.004			
Microlobulated margins (DBT + DM)	7.29 (2.32–22.85)	0.001			
Microcalcifications (DBT + DM)	2.98 (1.13–7.82)	0.027			

OR odds ratio, *CI* confidence interval, *DBT* digital breast tomosynthesis, *DM* digital mammography, *US* ultrasonography, *MRI* magnetic resonance imaging

Discussion

As a relatively new mammography technique, DBT is being promoted for clinical diagnosis, because DBT can better distinguish the mass lesion, architectural distortion, and spiculated margins [6, 9]. However, it is easier to observe the distribution of microcalcifications using DM. Therefore, we combine the two methods.

Moreover, there was no single imaging feature that can satisfactorily characterize different molecular subtypes. Therefore, the combination of multiple imaging (US, DBT + DM, MRI) may improve the accuracy of the expected diagnosis and increase the possibility of noninvasive pathologic diagnosis of breast cancer.

In this study, we analyzed the associations between imaging features and molecular subtypes of breast cancer in young women (≤30-year-old) and the results indicated

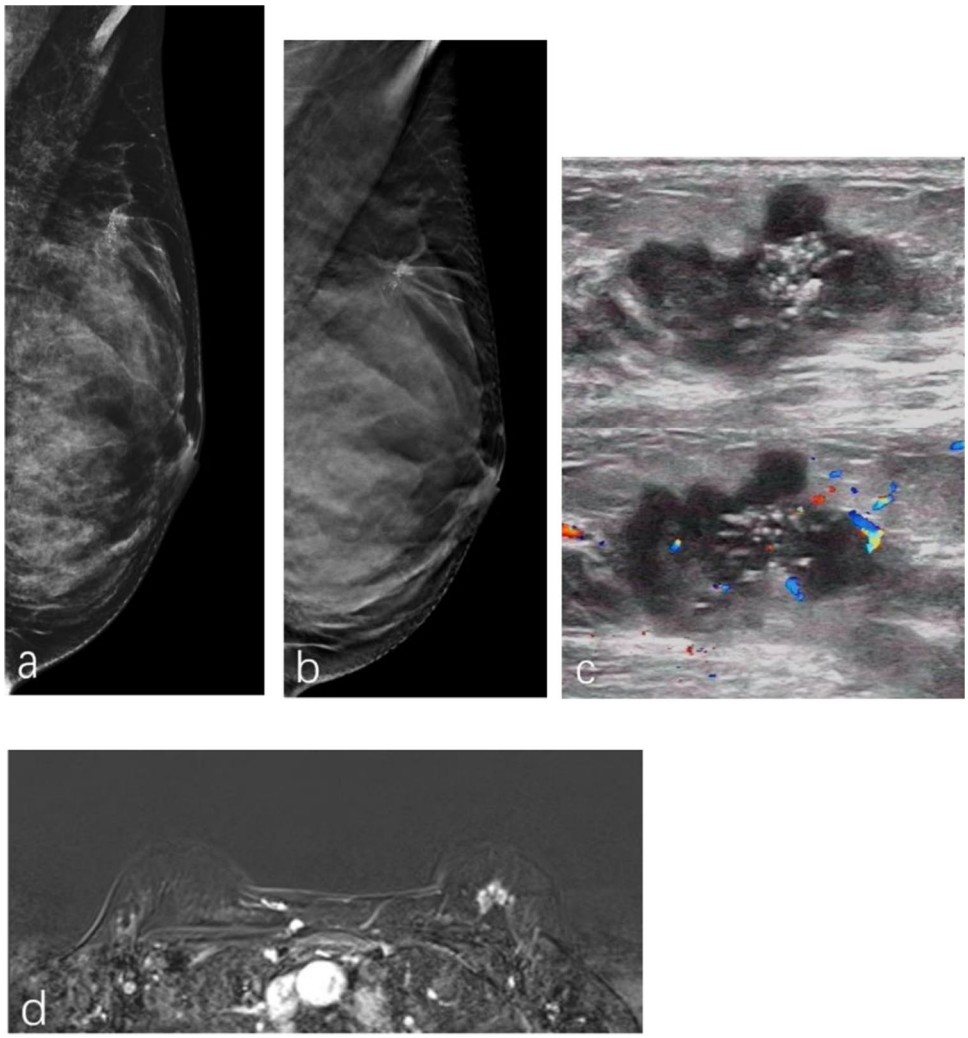

Fig. 1 A 29-year-old woman with invasive ductal carcinoma in the left breast, and molecular subtype is luminal B(HER2−) subtype. **a**, **b** DM + DBT (mediolateral view): irregular shape, spiculated margins, with fine pleomorphic calcifications (**b** shows spiculated margin clearer than in **a**). **c** Ultrasonography: irregular shape, angular margins, hypoechoic, shadowing posterior feature, with calcifications. **d** MR image: irregular shape, spiculated margins, heterogeneous enhancement

that certain imaging features were associated with specific molecular subtypes.

Compared to the general population (LB: 8.8%, LA: 61.8%), we found a greater proportion of young women with LB (45.9%) subtype (LB(HER2−): 30.6%, LB(HER2+): 15.3%) and a lesser proportion with LA subtype (21.8%) [13], and our results were similar to that of previous research about young women [6, 14, 15]. However, Ann et al. and Lin et al. studies [4, 13] concluded that the LA subtype was significantly more prevalent among young patients. Furthermore, our results had a higher prevalence of TN subtype (18.2%) than HER2-enriched subtype (14.1%), which was in line with some previous studies [4, 13, 14]. Contrary to these results, Bullier et al. [15] reported a higher prevalence of HER2-enriched subtype and a lower prevalence of TN subtype in young patients. The reason may be that the age group of the young patients we chose was different.

In our study, LB and LA subtypes showed a positive association with spiculated margins. The finding was similar to that of previous studies, which indicated that tumors with shadowing posterior features had a higher association with hormone receptor positivity [4, 15–17]. The presence of hormone receptor-positive status showed the stromal reaction, perilesional spiculations, and fibrosis resulting in shadowing posterior features and spiculated margins [16, 17]. Spicules were caused by the cancerous tissue which grows to infiltrate into the surrounding area, resulting in a high stromal reaction and fibrous connective tissue hyperplasia. This is an early protective mechanism, which can limit the spread of cancer cells to a certain extent. But, LB(HER2+) subtype showed more angular margins on ultrasound. This may be due to the ultrasonic statically collected images, which may lead to misinterpretation between the spiculated margins and the angular margins. Because few prior studies had investigated the LB(HER2+) subtype, this needed to be evaluated by a large sample later. In contrast to LA, LB(HER2+) had a higher vascularity. Previous studies indicated that HER2 overexpression was closely related to increased angiogenesis and expressed vascular endothelial growth factor (VEGF)

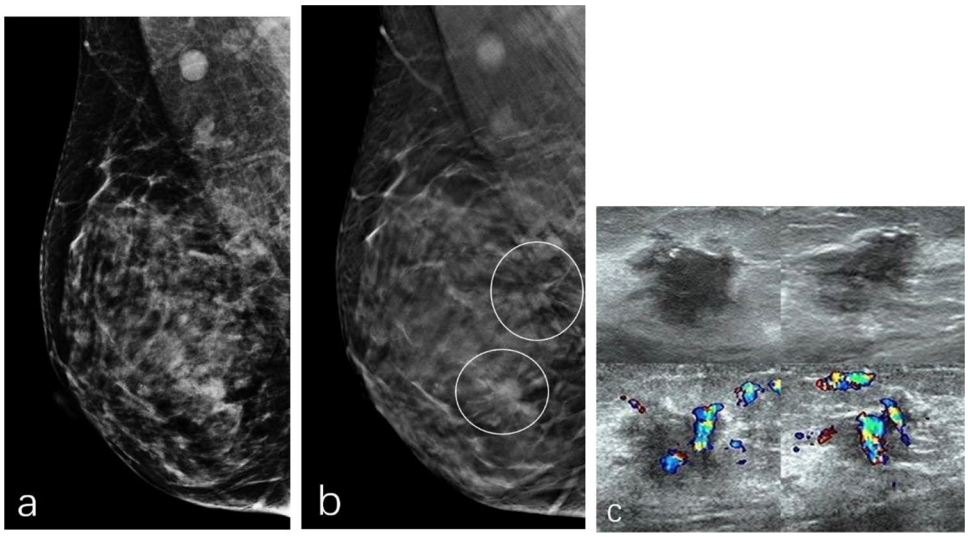

Fig. 2 A 30-year-old woman with invasive ductal carcinoma in the right breast, and molecular subtype is luminal B(HER2+) subtype. **a** DM (mediolateral view) showed an irregular shape, indistinct margins lesion. It did not detect the radial lesion seen on the DBT. **b** DBT (mediolateral view) (circle): a. irregular shape, spiculated margins, with amorphous microcalcification. **b** Irregular shape, spiculated margins lesion. **c** Ultrasonography: irregular shape, spiculated margins, hypoechoic, no posterior feature

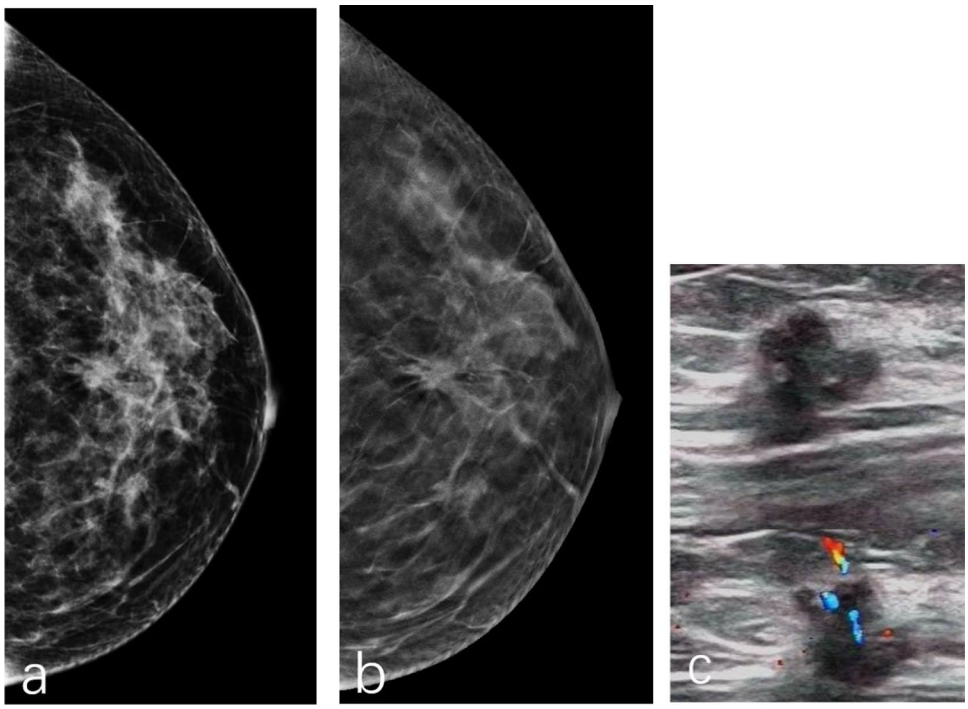

Fig. 3 A 29-year-old woman with invasive ductal carcinoma in the left breast, and molecular subtype is luminal A type. **a** DM (craniocaudal view) showed an irregular shape, indistinct margins lesion. **b** DBT (craniocaudal view) showed an irregular shape, spiculated margins lesion. **c** Ultrasonography showed an irregular shape, angular and spiculated margins, hypoechoic, shadowing posterior features

[18]. In addition, LB showed more mass with microcalcifications cases, and the presence of microcalcification may also cause shadowing posterior features. Missed diagnosis (no abnormality) often occurred in the LA subtype, which may be because LA was a low-grade tumor, with a relatively slow growth compared with the other four subtypes, and some lesions were small, so it was difficult to detect on mammography. Therefore, combining with multiple imaging examinations was more conducive to the diagnosis of diseases.

Previous studies showed that the expression of the HER2 was strongly correlated with the presence of calcification [4, 6, 15, 19]. It might account for the frequent observation of microcalcification in the HER2-enriched subtype. Our results were consistent with this. It was confirmed by pathology that the microcalcification seen by mammography in young patients was related to the intraductal carcinoma [20]. This may be caused by the high cell turnover and insufficient blood supply, so malignant calcifications often manifested as necrosis. This may explain the intraductal components that usually appear in the form of microcalcifications. These calcifications were characterized by fine linear, linear branching or coarse heterogeneous patterns,

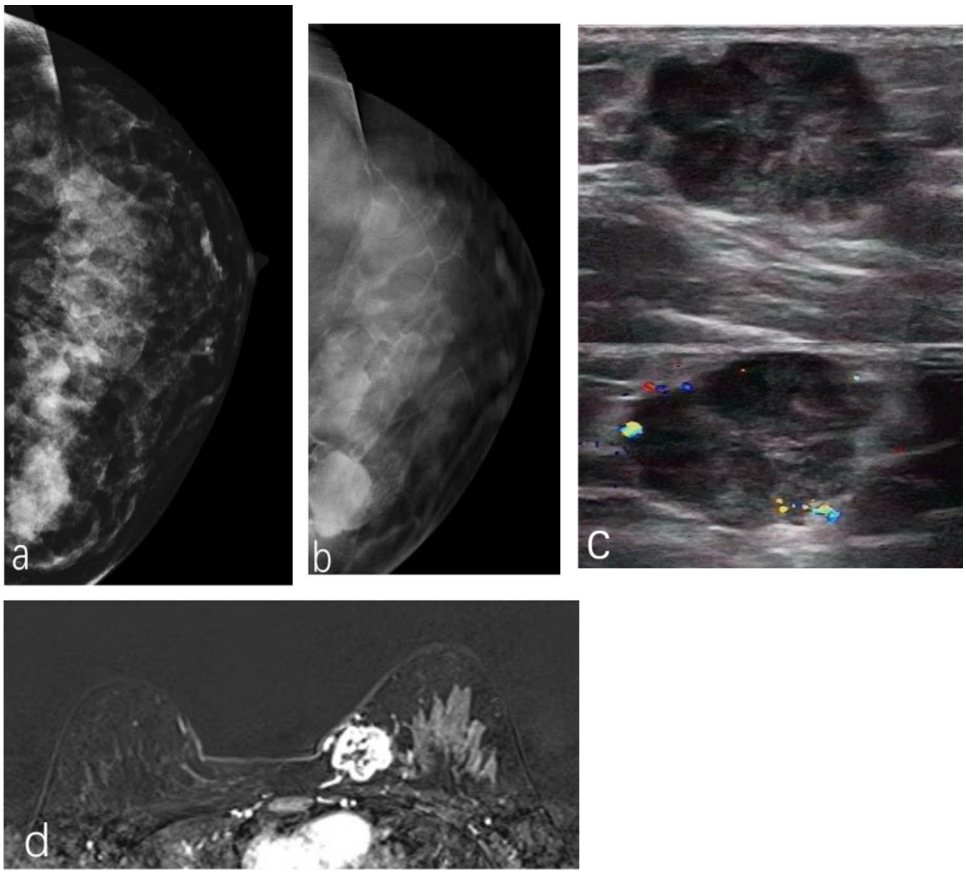

Fig. 4 A 28-year-old woman with invasive ductal carcinoma in the left breast, and molecular subtype is TN subtype. **a** DM (craniocaudal view): irregular shape, indistinct margins. **b** DBT (craniocaudal view): oval shape, circumscribed margins. **c** Ultrasonography: irregular shape, circumscribed and lobulated margins, hypoechoic, enhancement of posterior feature. **d** MR image: oval shape, irregular margins, rim enhancement

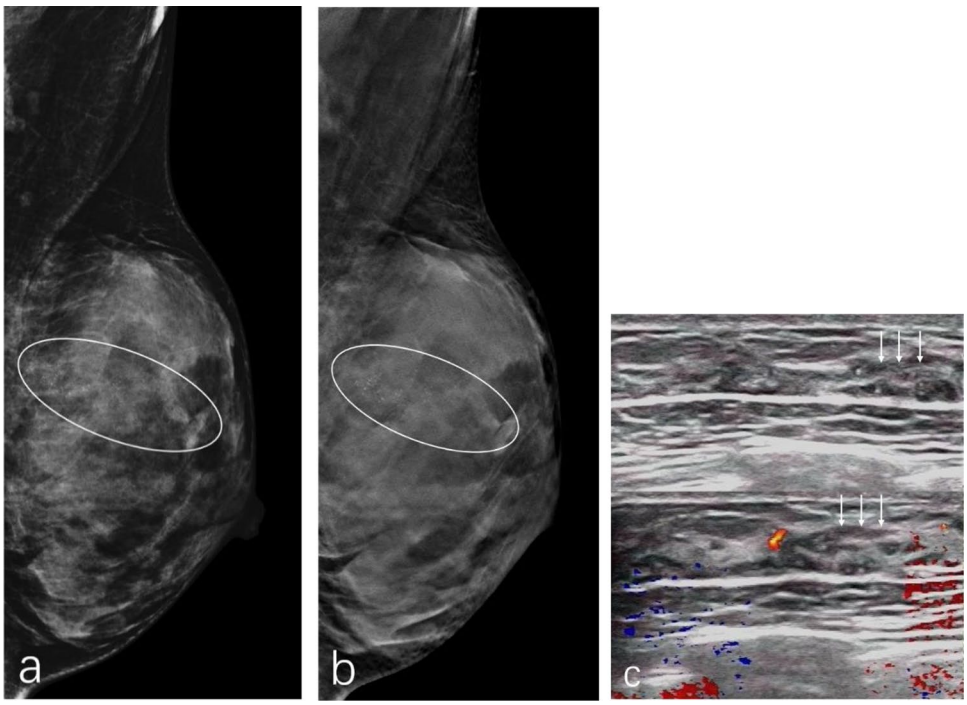

Fig. 5 A 26-year-old woman with ductal carcinoma in situ in the left breast, and molecular subtype is HER-2 enriched subtype. **a**, **b** DM + DBT (mediolateral view): segmental fine linear and pleomorphic microcalcifications. **c** Ultrasonography: intraductal calcifications (arrows)

Table 5 Agreement between two radiologists in terms of imaging features

	Read 1 lesions, *n*	Read 2 lesions, *n*	Discordant cases		Kappa value (95% CI)
			R1 vs R2	R2 vs R1	
US					
Shape (mass)					
Oval/round	46	45	4	3	0.89 (0.81–0.97)
Irregular	99	100	3	4	
Margins (mass)					
Circumscribed	20	18	3	1	0.89 (0.84–0.95)
Indistinct	36	35	1	–	
Microlobulated	18	21	1	4	
Spiculated	47	44	5	2	
Angular	24	27	2	5	
Echogenicity					
Hypoechoic	91	90	5	4	0.88 (0.79–0.96)
Heterogenous	47	48	4	5	
Complex cystic and solid	7	7	–	–	
Posterior feature					
No	45	47	2	4	0.91 (0.85–0.97)
Enhancement	24	23	1	–	
Shadowing	61	57	6	2	
Combined	15	18	–	3	
DBT + DM					
Breast density					
a, b	16	18	2	1	0.92 (0.86–0.97)
c, d	152	150	1	2	
Shape (for mass)					
Oval/round	35	34	2	1	0.94 (0.88–1.00)
Irregular	98	99	1	2	
Margins (for mass)					
Circumscribed	19	20	–	1	0.93 (0.88–0.98)
Indistinct	22	21	3	2	
Microlobulated	22	22	3	3	
Spiculated	70	70	–	–	
Hyper	72	73	1	2	0.96 (0.90–1.00)
Iso	61	60	2	1	
Amorphous	1	3	–	2	0.81 (0.62–0.99)
Fine pleomorphic or coarse heterogeneous	12	9	3	–	
Fine linear or linear branching	16	17	–	1	
Diffuse	3	3	–	–	0.85 (0.70–1.00)
Regional	5	6	1	2	
Grouped	9	8	2	1	
Linear/segmental	12	12	–	–	
MRI					
Shape (mass)					
Oval/round	8	9	1	2	0.76 (0.51–1.00)
Irregular	25	24	2	1	
Margins (mass)					
Circumscribed	8	6	2	–	091 (0.78–1.00)
Irregular	10	12	–	2	
Spiculated	15	15	–	–	

Table 5 (continued)

	Read 1 lesions, *n*	Read 2 lesions, *n*	Discordant cases		Kappa value (95% CI)
			R1 vs R2	R2 vs R1	
Enhancement (mass)					
Homogenous	3	5	–	2	0.88 (0.73–1.00)
Heterogenous	22	20	2	–	
Rim	8	8	–	–	
Distribution (NME)					
Focal/regional	3	2	1	–	0.76 (0.39–1.00)
Linear/segmental	5	5	–	–	
Diffuse	0	1	–	1	
Enhancement (NME)					
Heterogenous	1	1	–	–	0.74 (0.28–1.00)
Clumped	6	5	1	–	
Clustered ring	1	2	–	1	

DBT digital breast tomosynthesis, *DM* digital mammography, *US* ultrasonography, *MRI* magnetic resonance imaging, *NME* non-mass enhancement

and our results were similar. Therefore, the value of mammography in young women for breast cancer may increase. In addition, the HER2-enriched subtype was found to be a high-grade tumour. High-grade tumour had more cellular features, which can lead to the reduced attenuation of the ultrasound waves, thus presented as the enhancement posterior features [21]. In consideration of the above two reasons, the HER2-enriched subtype frequently presented a combined posterior feature on ultrasound. Previous studies [18] showed that the HER2-enriched subtype is a high vascular lesion. However, there were more high vascular lesions than low vascular lesions in our study, which was not statistically significant. The possible reason was that the number of cases was small, which needed to be verified in a later large sample later. Furthermore, HER2-enriched subtype often showed microlobulated margins, which were similar to Bullier's research [15].

As reported in prior studies [22–24], TN subtype often presented well-defined benign imaging features such as oval/round shape, circumscribed margins, no microcalcifications, as well as a higher necrotic portion that yielded high T2-weighted signal intensity on MRI and enhancement of posterior feature on US imaging. Moreover, Uematsu et al. [24] suggested that rim enhancement was an important independent predictor of higher histological grade and negative hormone receptor expression. Our result was consistent with this. Furthermore, our study showed that the TN subtype had less vascular than the HER2-enriched subtype, which may be due to the higher cellularity and necrosis [8, 25]. So, it is important to carefully evaluate the margins and vascularity of tumor to avoid a missed diagnosis in this situation.

This study had several limitations. First, this was a retrospective study, and the sample size was not enough because breast cancer in young women under the age of 30 years was rare. Second, the MRI sample size was small, which may weaken the statistical power of the results. A multicenter prospective study with a large sample needs to be performed to validate the present results.

Conclusion

Compared with the general population of breast cancer, this young female population presents a different molecular phenotype distribution. Certain imaging features may be associated with specific breast cancer molecular subtypes in young women ≤30 years old. The mass (with microcalcifications) lesions with spiculated margins and shadowing posterior features were predicted to be LB subtypes. If it was accompanied by high vascularity in US, it was likely to be the LB(HER2+) subtype; otherwise, it tended to be the LB(HER2−) subtype. The only mass lesions with spiculated margins, shadowing posterior features, and low vascularity were predicted to be LA subtypes. Tumors with isolated microcalcification or mass with microlobulated margins, combined posterior features, and high vascularity were strongly predicted to be HER2-enriched subtype. Circumscribed margins of mass with an oval or round shape, enhancement of posterior features, and rim enhancement (MRI) were strongly predicted to be TN subtype.

Funding The authors did not receive any financial support for the research, authorship and/or publication of this article. National Key Research and Development Programme of China (Grant No. 2016YFC 1303004).

Compliance with ethical standards

Conflict of interest The authors declare that they have no conflict of interest.

References

1. Limbach KE, Leon E, Pommier RF, Pommier SJ. Comparison of breast cancer incidence, clinicopathologic features, and risk factor prevalence in women aged 20–29 at diagnosis to those aged 30–39. Breast J. 2020;26:1069–70.
2. Thomas A, Rhoads A, Pinkerton E, Schroeder MC, Conway KM, Hundley WG, et al. Incidence and survival among young women with stage I-III breast cancer: SEER 2000–2015. JNCI Cancer Spectr. 2019;3:pkz040.
3. Hamilton LJ, Cornford EJ, Maxwell AJ. A survey of current UK practice regarding the biopsy of clinical and radiologically benign breast masses in young women. Clin Radiol. 2011;66:738–41.
4. An YY, Kim SH, Kang BJ, Park CS, Jung NY, Kim JY. Breast cancer in very young women (<30 years) imaging features with clinicopathological features and immunohistochemical subtypes. Eur J Radiol. 2015;84:1894–902.
5. Li H, Zheng RS, Zhang SW, Zeng HM, Sun KX, Xia CF, et al. Incidence and mortality of female breast cancer in China, 2014. Zhonghua Zhong Liu Za Zhi. 2018;40:166–71.
6. Cai Q, Yao M, Cai D, Zeng HM, Sun KX, Xia CF, et al. Association between digital breast tomosynthesis and molecular subtypes of breast cancer. Oncol Lett. 2019;17:2669–766.
7. Murphy BL, Day CN, Hoskin TL, Habermann EB, Boughey JC. Adolescents and young adults with breast cancer have more aggressive disease and treatment than patients in their forties. Riv Psichiatr. 2019;54:160–7.
8. Durhan G, Azizova A, Önder Ö, Kösemehmetoğlu K, Karakaya J, Akpınar MG, et al. Imaging findings and clinicopathological correlation of breast cancer in women under 40 years old. Eur J Breast Health. 2019;15:147–52.
9. Phi XA, Tagliafico A, Houssami N, Greuter MJW, de Bock GH. Digital breast tomosynthesis for breast cancer screening and diagnosis in women with dense breasts—a systematic review and meta-analysis. BMC Cancer. 2018;18:380.
10. American College of Radiology. Breast imaging and reporting and data system (ACR BI-RADS® Atlas). 5th ed. USA: American College of Radiology; 2013.
11. Coates AS, Winer EP, Goldhirsch A, Gelber RD, Gnant M, Piccart-Gebhart M, et al. Tailoring therapies—improving the management of early breast cancer: St Gallen International Expert Consensus on the primary therapy of early breast cancer 2015. Ann Oncol. 2015;26:1533–46.
12. Seigel DG, Podgor MJ, Remaley NA. Acceptable values of kappa for comparison of two groups. Am J Epidemiol. 1992;135:571–8.
13. Lin CH, Liau JY, Lu YS, Huang CS, Lee WC, Kuo KT, et al. Molecular subtypes of breast cancer emerging in young women in Taiwan: evidence for more than just westernization as a reason for the disease in Asia. Cancer Epidemiol Biomark Prev. 2009;18:1807–14.
14. Collins LC, Marotti JD, Gelber S, Cole K, Ruddy K, Kereakoglow S, et al. Pathologic features and molecular phenosubtype by patient age in a large cohort of young women with breast cancer. Breast Cancer Res Treat. 2012;131:1061–6.
15. Bullier B, MacGrogan G, Bonnefoi H, Hurtevent-Labrot G, Lhomme E, Brouste V, et al. Imaging features of sporadic breast cancer in women under 40 years old: 97 cases. Eur Radiol. 2013;23:3237–45.
16. Irshad A, Leddy R, Pisano E, Baker N, Lewis M, Ackerman S, et al. Assessing the role of ultrasound in predicting the biological behavior of breast cancer. AJR Am J Roentgenol. 2013;200:284–90.
17. Taneja S, Evans AJ, Rakha EA, Green AR, Ball G, Ellis IO. The mammographic correlations of a new immunohistochemical classification of invasive breast cancer. Clin Radiol. 2008;11:1228–355.
18. Zhang L, Li J, Xiao Y, Cui H, Guoqing Du, Wang Y, et al. Identifying ultrasound and clinical features of breast cancer molecular subtypes by ensemble decision. Sci Rep. 2015;5:11085.
19. Kim SH, Seo BK, Lee J, Kim SJ, Cho KR, Lee KY, et al. Correlation of ultrasound findings with histology, tumor grade, and biological markers in breast cancer. Acta Oncol. 2008;47:1531–8.
20. Hermann G, Janus C, Schwartz IS, Papatestas A, Hermann DG, Rabinowitz JG. Occult malignant breast lesions in 114 patients: relationship to age and the presence of microcalcifications. Radiol. 1988;169:321–4.
21. Lamb PM, Perry NM, Vinnicombe SJ, Wells CA. Correlation between ultrasound characteristics, mammographic findings and histological grade in patients with invasive ductal carcinoma of the breast. Clin Radiol. 2000;55:40–4.
22. Boisserie-Lacroix M, Macgrogan G, Debled M, Ferron S, Asad-Syed M, McKelvie-Sebileau P, et al. Triple-negative breast cancers: associations between imaging and pathological findings for triple-negative tumors compared with hormone receptor-positive/human epidermal growth factor receptor-2-negative breast cancers. Oncologist. 2013;18:802–11.
23. Youk JH, Son EJ, Chung J, Kim JA, Kim EK. Triple-negative invasive breast cancer on dynamic contrast-enhanced and diffusion-weighted MR imaging: comparison with other breast cancer subtypes. Eur Radiol. 2012;22:1724–34.
24. Uematsu T, Kasami M, Yuen S. Triple-negative breast cancer: correlation between MR imaging and pathologic findings. Radiol. 2009;250:638–47.
25. Kojima Y, Tsunoda H. Mammography and ultrasound features of triple-negative breast cancer. Breast Cancer. 2011;18:146–51.